Advanced Simulation and History Matching Approaches on WAG Experiments in High-Permeability Reservoir Cores

Gilles Puyou[1], *Marcel* Bourgeois[1], *Cyril* Caubit[1]

[1] TotalEnergies OneTech, Pau, France

Abstract. This paper presents a comprehensive study of Water Alternating Gas (WAG) injections in highly permeable reservoir samples, focusing on advanced simulation workflows and history matching methodologies. The experimental program was designed to explore the effects of gravity-driven flows and thermodynamic interactions between gas and oil, focusing on phenomena like stripping, swelling, and changes in petrophysical properties. Careful monitoring of effluent volumes and composition provided a comprehensive dataset for effective simulation and interpretation. A key contribution of this work is the application of a simulation workflow specifically adapted to the experimental context, highlighting the importance of the fluid Equation of State and simulation grid configuration (grid size, completion strategy, kv/kh ratios). The use of X-ray data proved crucial for understanding fluid distribution and flow dynamics, ensuring accurate modeling of physical processes. The study systematically compares several history-matching techniques, including the use of Residual Oil saturation (SOR) keyword and Alpha-Factors transport coefficients. These respectively constrain oil evaporation at the grid cell level and modulate gas-oil compositional exchanges. Three-phase WAG models, including the Land parameter, gas and water mobility reduction, are refined by integrating water trapping parameters. In addition, a sensitivity analysis is performed where the gas-oil interactions are weakened by departing from the usual full mixing assumption, thus reproducing better the observed compositions. Special attention is given to the challenges in very permeable environments, where pressure responses and phase transitions interplay with gravity. Incorporating dead volumes into history matching improves the calibration of simulations against experimental results. The study includes a case example illustrating the interpretation and history matching of a long-slug WAG test, which starts with gas injection followed by alternating cycles of water and gas. This example demonstrates the non-uniqueness of history matching results and emphasizes that each technique has its own strengths and limitations depending on experimental and reservoir conditions. Overall, the study underscores the fundamental role of gravity effects and thermodynamic interactions in stabilizing the gas front and improving recovery efficiency during WAG injection. The presented workflow offers valuable tools for interpreting experimental data and optimizing field WAG operations, improving the understanding of multiphase flow and supporting the application of advanced simulation and history matching in high-permeability reservoirs.

1 Introduction

Water Alternating Gas (WAG) injection remains one of the most widely deployed enhanced oil recovery (EOR) processes to improve macroscopic sweep efficiency, particularly in high-permeability reservoirs where gravity segregation and viscous instabilities strongly control displacement efficiency (Egermann et al., [1]). These challenges are exacerbated in offshore settings, where gravity-driven mechanisms dominate recovery performance and critically impact field-scale efficiency (Pizarro et al., [2]). Recent large-scale offshore developments further emphasize the strategic role of gravity-stabilized gas-based recovery processes in modern EOR portfolios (Burns et al., [3]).

Despite decades of field experience, the predictive capability of WAG processes remains limited by the difficulty in reliably parameterizing three-phase relative permeabilities and trapping mechanisms, especially under miscible conditions. In such conditions, injected gas and reservoir oil partially or fully mix at the pore scale. This mixing reduces interfacial tension and significantly alters displacement behavior.

While these mechanisms have long been recognized as key controls on WAG performance (Skauge and Larsen, [4]), their quantification from laboratory data remains highly uncertain. In particular, history matching of WAG coreflood experiments is intrinsically non-unique: multiple parameter sets and modeling strategies can reproduce the same experimental observables, leading to significantly different interpretations and predictive outcomes.

The renewed industrial interest in gas-based EOR further emphasizes the need for robust laboratory interpretation workflows capable of supporting large-scale deployment (Bourgeois et al., [5]).

Over the years, several history matching methodologies have been proposed in the literature, relying on different levels of data integration (pressure, production, in-situ saturation), weighting strategies, and parameterization schemes. However, no clear consensus has emerged regarding their relative robustness and efficiency, especially when confronted with rich experimental datasets including spatial saturation measurements.

* Corresponding author: gilles.puyou@totalenergies.com

This paper addresses this gap by presenting the interpretation of a WAG coreflood program conducted on high-permeability sandstone cores, combining pressure drops, phase production, effluent compositions, and in-situ saturation maps obtained from X-ray monitoring. Beyond deriving a consistent set of two- and three-phase flow parameters through advanced simulation and multi-objective history matching, the core objective of this study is to systematically evaluate and compare several history matching methodologies reported in the literature. By applying these approaches to the same comprehensive dataset, this work aims to identify the most effective and robust workflow, ensuring consistency between dynamic responses and saturation distributions, and reducing interpretation uncertainty.

2 Experimental backgrounds

Four WAG coreflood experiments were performed at high pressure and high temperature (HPHT) using live oil, synthetic formation brine, and a recombined injection gas. All the experimental work of this program was previously presented in detail by Puyou et al. [6]. The present paper focuses exclusively on the interpretation of that dataset and therefore constitutes the continuation and extension of this previous study.

The experimental program described in Puyou et al. [6] includes both long-slug and short-slug WAG sequences (Duchenne et al. [7], Joubert et al. [8]), carried out in horizontal and vertical core orientations to isolate gravity effects.

Additionally, two experiments performed under lighter conditions (10 bar and 90°C, using dead oil, synthetic water, and gas) were designed to constrain the water/oil and gas/oil relative permeability curves. These complementary tests were also used to anchor the capillary pressure functions.

Figure 1 summarizes the full set of HPHT experiments and highlights the main results in terms of saturation changes as a function of WAG cycle progression. No additional experiments are presented in this work; the contribution lies entirely in the interpretation and advanced analysis of the existing dataset.

Production was monitored at reservoir and surface conditions for material balance, while a dedicated 2D X-ray system provided saturation maps (Savin et al. [9]). Gravity-driven segregation patterns are highlighted by the WAG1a horizontal gas slugs, where gas preferentially migrates to the top of the core.

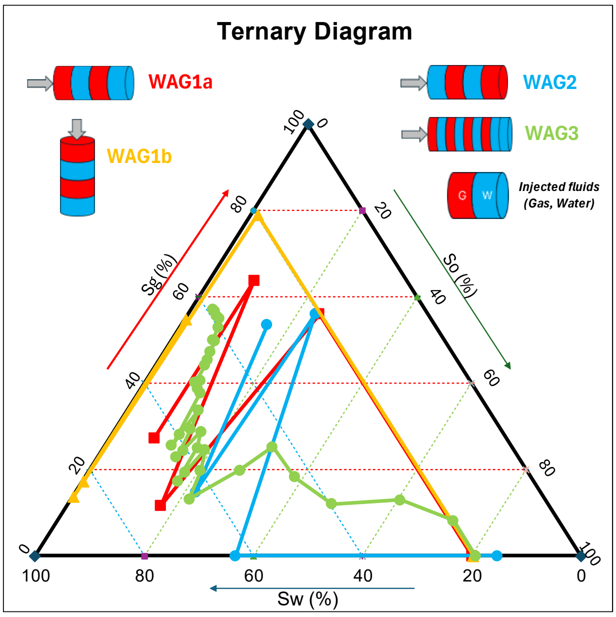

Figure 1 - *Comparison of the full WAG program saturation changes on a ternary diagram*

3 Numerical interpretation frameworks

3.1 Intersect and relative permeability model

Numerical interpretation was carried out using the compositional reservoir simulator Intersect (IX). Three-phase flow behavior was modeled using the Larsen–Skauge WAG hysteresis formulation (IX keyword: WAGhysteresis), accounting for gas trapping, gas mobility reduction due to cyclic water injection, and water mobility reduction in the presence of gas.

In all cases, hysteresis effects were described using the Killough hysteresis formulation for relative permeability scanning curves (Killough, [10]).

Three variants of the WAG hysteresis model were evaluated: (i) the conventional formulation, (ii) an improved formulation allowing distinct two- and three-phase water relative permeability curves, and (iii) an extended formulation incorporating explicit water trapping through a Land-type approach.

(i) Conventional WAG hysteresis model (Larsen and Skauge, [11]):
No additional hysteresis is introduced on Krw beyond the Killough formulation. The model distinguishes between Krw2φ (two-phase water/oil, no gas) and Krw3φ (three-phase, presence of gas). Interpolation between these curves is controlled by Sgstart, which represents the gas saturation at the onset of imbibition (Sw increasing). Both curves share the same shape and are proportional, with Krw3φ = Krw2φ / Rkw, where Rkw is the water relative permeability reduction factor (Figure 2).

(ii) Improved WAG hysteresis model (Shahverdi and Sohrabi [12], Bourgeois et al. [13]):

Krw3φ has a different shape from Krw2φ. It is controlled by hard-coded Swt (trapped water saturation) values (Figure 2). Interpolation between Krw2φ and Krw3φ remains governed by Sgstart.

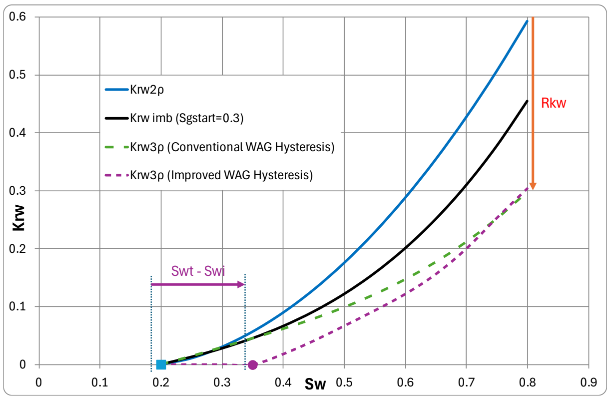

Figure 2 - *Water relative permeability models in 3-phase for conventional and improved WAG hysteresis*

(iii) Extended WAG hysteresis model (Land [14]):
This formulation enforces multi-cycle consistency in Krw hysteresis. Krw2φ represents the imbibition curve, while Krw3φ corresponds to the drainage curve. The drainage process terminates at a trapped water saturation Swt, determined from Cw and the maximum water saturation Swmax reached at the onset of gas injection, following Land's approach. During tertiary waterflooding, interpolation between Krw2φ and Krw3φ is controlled by Swstart instead of Sgstart.

3.2 Grid design and gravity representation

Because of very high permeability and strong segregation, horizontal experiments were interpreted using two-dimensional grids to reproduce vertical segregation, while the vertically oriented experiment was interpreted using a one-dimensional grid.
Sensitivity analyses were conducted on key modeling parameters, including the vertical-to-horizontal permeability ratio (kv/kh) and well completion strategies. Sensitivity analysis is a standard approach in reservoir simulation to quantify the impact of uncertain parameters and to identify those controlling the model response prior to calibration (Heidari et al., [15]). These analyses demonstrated that accurate reproduction of X-ray saturation profiles requires an explicit representation of gravity effects before parameter tuning.
A two-dimensional Cartesian grid was therefore employed, consisting of 50 cells in the horizontal direction, with cell dimensions consistent with the core length and assuming homogeneous porosity and permeability properties. This level of spatial discretization is necessary to capture multi-directional flow and segregation phenomena that cannot be represented in simplified one-dimensional models.
Kv/Kh values were tested and checked in comparison with X-ray saturation calculations (Figure 3).

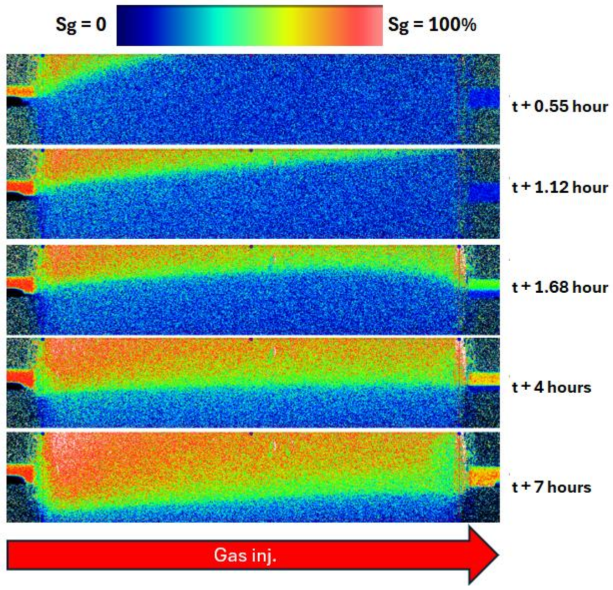

Figure 3 - *Saturation change observations with X-ray measurements during first gas injection. Injection from left to right. Red means 100% of gas saturation and blue 0%*

Figure 4 shows that Kv/Kh lower than 1 underestimates saturation variation, reflecting insufficient vertical communication. In contrast, Kv/Kh greater than 1 reproduces the observed behavior, highlighting the role of gravity-driven flow. Based on this sensitivity analysis, a value of Kv/Kh = 1 was retained for this study as a balanced representation of vertical and horizontal permeability effects.

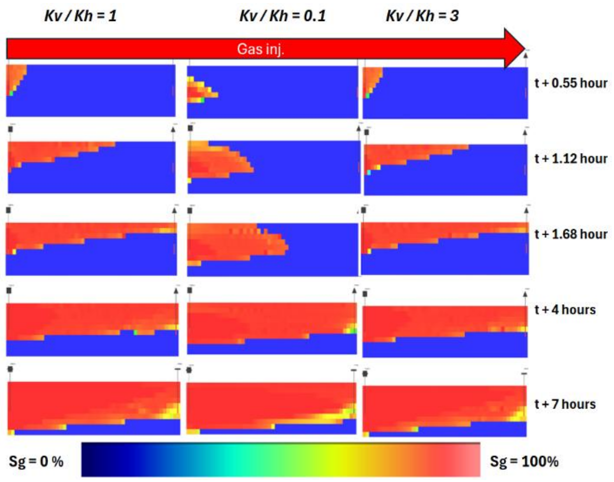

Figure 4 - *Saturation change observations on simulations depending on Kv/Kh. Injection from left to right. Red means 100% of gas saturation and blue 0%. Same range than X-ray value in Figure 3*

Wells were positioned in the first X cell (injection well) and the last X cell (production well). The injection well alternates between being a gas injector and a water injector depending on the phase of the WAG experiment. Completions were established following a quality control of the saturation changes observed with 2D X-Ray measurement (Figure 3). The impact on the size of the completion is significant only in horizontal experiment interpretations. The injector is connected to the middle of the height of the core in only one cell, whereas the production well is connected across two cells.

Two saturation regions were defined. The first one (global region) includes all petrophysical and three-phase parameters, with capillary pressure curves derived from the 1D interpretation of the HPHT waterflood and complemented by light-condition data for the gas–oil system. The second region, located near the outlet (last X cells), represents capillary end effects. It uses identical properties but assumes Pc = 0.

4 Equation of State and gas–oil interaction

A simplified compositional Equation of State (EOS) with 10 pseudo-components was adopted for this study. This model provides a good balance between physical representativeness and computational efficiency.
The EOS was calibrated and validated against laboratory PVT data, including viscosity, density, and formation volume factor (Bo) (Figures 5 and 6).

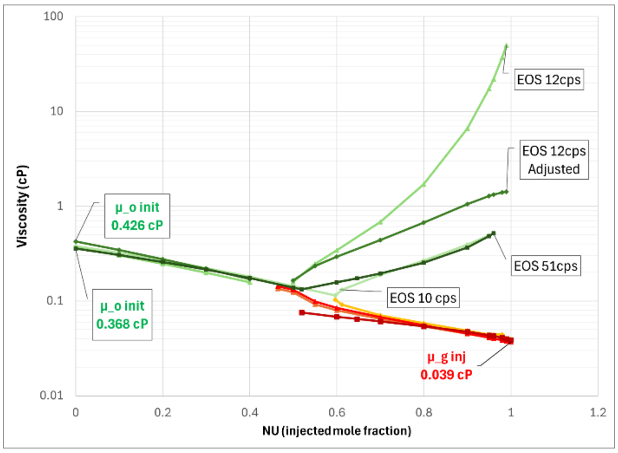

Figure 5 - *G/O interaction impact on viscosity for various versions of EOS. Validation of the retained 10 pseudo-component EOS against viscosity trends.*

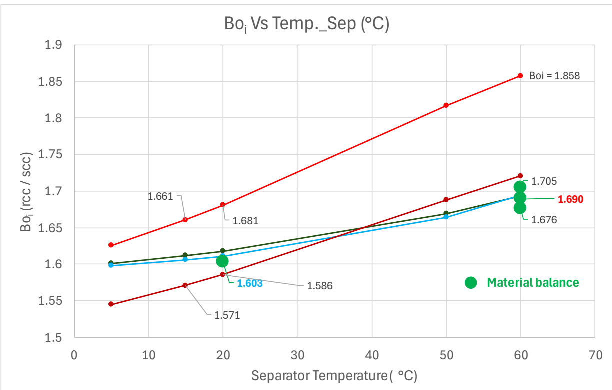

Figure 6 - *Initial Bo evolution versus temperature for the various versions of EOS*

Particular attention was paid to gas–oil interactions under near-miscible conditions. An initial formulation led to excessive swelling and unrealistic viscosity variations during gas injection. The EOS was therefore adjusted to better reproduce laboratory behavior, resulting in improved predictions of both viscosity and Bo.
The final 10-component EOS was retained as it ensures a realistic description of multi-contact miscibility while remaining consistent with experimental observations.

5 History matching methodology

5.1 Objective function and data constraints

The history matching process aims to identify model parameters that minimize an objective (cost) function quantifying the mismatch between simulated and observed data. In this study, the objective function includes cumulative oil, water, and gas production, differential pressure, in-situ saturation profiles from X-ray monitoring, and effluent compositions (Duchenne et al. [16]). The diversity and complementarity of these measurements are critical to constrain the solution. Matching production data alone is insufficient to ensure consistency with saturation distributions and compositional trends.
The integration of this extended dataset significantly reduces the non-uniqueness of the solution by enforcing consistency across multiple physical responses.

5.2 Two-phase relative permeability

Gas–oil and oil–water relative permeabilities were derived from WAG experiments, using the first injection cycle of each sequence.

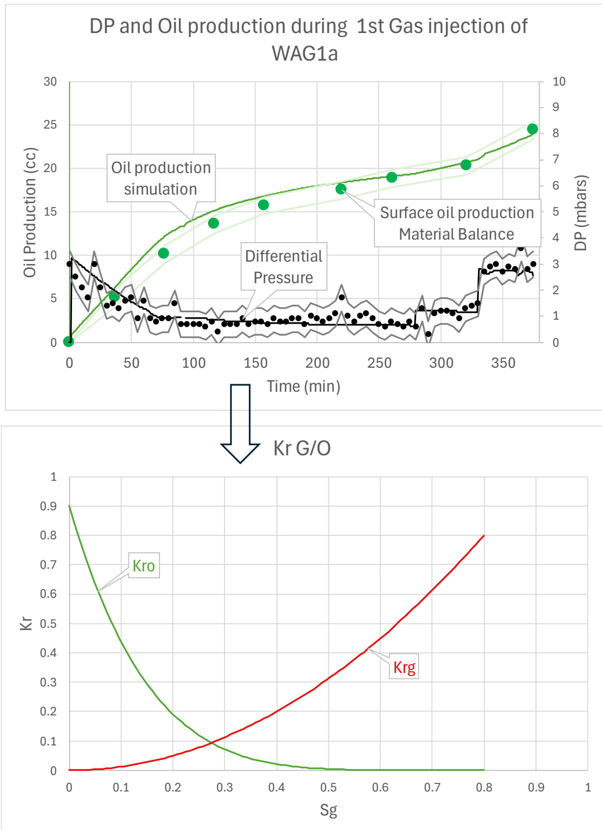

Figure 7 - *Two phases' sequences history matched for Kr G/O*

For WAG sequences starting with gas injection, gas–oil relative permeabilities were determined from the initial gas injection (Figure 7), during which gas displaces oil at reservoir conditions. This consists of history matching of the material balance data considering their uncertainties.

Conversely, for WAG sequences starting with water injection, oil–water relative permeabilities were determined from the first water injection, corresponding to the displacement of oil by water (Figure 8).

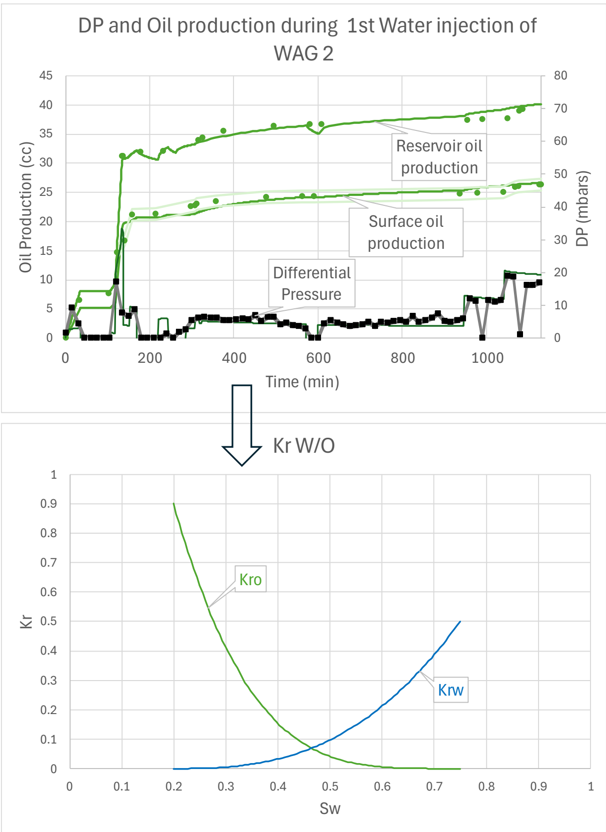

Figure 8 - *Two phases' sequences history matched for Kr W/O*

In both cases, the first injection cycle is considered representative as it precedes any significant hysteresis effects induced by cyclic injection.

Relative permeabilities were interpreted assuming monotonic saturation evolution during the first injection and negligible capillary end effects over the stabilized flow periods. The derived relative permeability curves reflect the effective flow behavior of the corresponding fluid pairs under multiphase displacement conditions typical of WAG processes.

To improve robustness and assess consistency, the gas–oil and oil–water relative permeability curves obtained at reservoir conditions were consolidated with additional experiments performed at light conditions (10 bar and 90 °C). These complementary tests were used to verify the internal consistency of the relative permeability trends and to constrain curve shapes across pressure and temperature ranges. The consolidation of datasets allowed the construction of representative relative permeability functions suitable for use in reservoir simulation, while preserving the physical coherence of gas–oil and oil–water flow behavior observed during WAG injection.

Relative permeability functions must first be selected to represent the dominant displacement mechanisms during WAG injection. Once these flow properties are defined, capillary pressure scaling is required to ensure consistency of fluid distribution and saturation functions between laboratory and reservoir conditions.

5.3 Capillary pressure consistency

Relative permeability curves are paired with capillary pressure descriptions using a log(β) formulation (Figure 9) for imbibition Pcow, anchored by saturation-at-zero-Pc constraints derived from outlet capillary end effects. This ensures consistency between pressure response and saturation profiles.

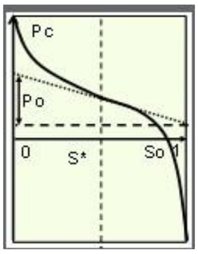

$$P_c = a.P_0.\ln\frac{(1 - S^{*\beta})}{S^{*\beta}} - \text{b}$$

Figure 9 - *Pc curve description*

Capillary pressure is primarily controlled by interfacial tension, following the Young-Laplace relationship. For a given rock, pore structure and wettability are assumed constant, so Pc variations between laboratory and reservoir conditions are dominated by changes in interfacial tension.

Accordingly, capillary pressure curves are scaled using the ratio of interfacial tensions evaluated at laboratory and reservoir conditions. At identical fluid saturation, the scaled capillary pressure is expressed as:

$$P_c^{HP/HT}(S) = P_c^{LP/LT}(S) \times \frac{\sigma_{HP/HT}}{\sigma_{LP/LT}} \quad (1)$$

where $P_c^{LP/LT}(S)$and $P_c^{HP/HT}(S)$ are the capillary pressures at a given saturation S under laboratory and reservoir conditions, respectively, and $\sigma_{LP/LT}$and σ_{HPHT} are the corresponding oil–water interfacial tensions.

This approach preserves the shape of the Pc curve while adjusting its magnitude to represent in-situ conditions.

5.4 Three-phase parameterization

The key adjustable three-phase parameters include the gas trapping coefficient (Cg) based on Land's formulation (Land [14]), the secondary drainage gas mobility reduction factor (αg) associated with cycle-dependent hysteresis (Larsen and Skauge [11]), the water mobility reduction factor in the presence of gas (Rkw) reflecting three-phase flow effects (Larsen and Skauge [11]), and the water trapping coefficient (Cw) introduced in extended WAG hysteresis formulations (Mahzari and Sohrabi [17]).

A zero-dimensional SCAL approach (0D) was performed to evaluate roughly three-phase parameters. This simplified interpretation uses core-averaged measurements. It helps to characterize the following:

- Relative permeability data at a given saturation by applying Darcy law on the measured Differential Pressure (DP) and the injection rates. The 0D approach is applied at the end of each slug. By comparing the 0D data of the different slugs, valuable information is obtained about the three phase parameters: Rkw (water mobility reduction) and αg (gas mobility reduction).
- Land parameter Cg can be obtained on the gas trapped saturation versus maximum gas saturation plot by matching the observed gas saturations using a Land function.
- Comparing the injectivity index evolution of long slugs allows to evaluate the front stabilization.

Figure 10 shows the conventional Land plot for gas: the trapped gas saturation during a water slug is an increasing function of the maximum gas saturation reached during the previous gas slug, which is traditionally called Sgm.

To determine Cg, the parameter controlling the trapped gas saturation (Sgt), it is necessary to plot the pairs of Sgt/Sgm calculated at the end of each stage during the long slug experiments.

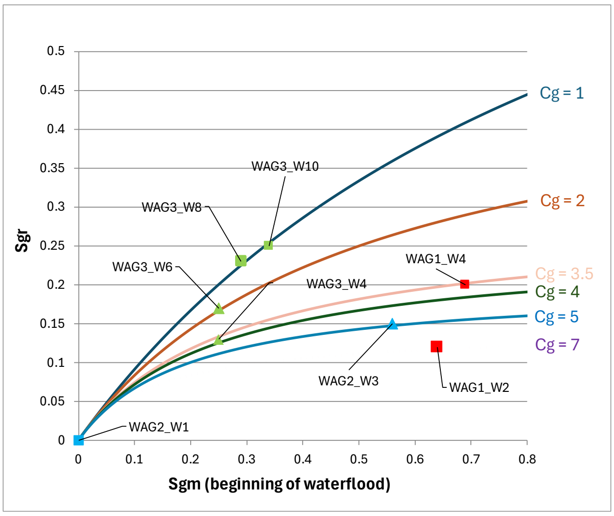

Figure 10 – *Estimation of Cg from WAG1A, WAG2 and WAG3 on the Sgt/Sgm plot. Symbols represent endpoint values derived from material balance, while solid lines correspond to the Land trapping model.*

The correlation coefficient is Cg, which is a Land coefficient for gas: the lower Cg, the higher Sgt.

$$C_g = \frac{1}{S_{gt}} - \frac{1}{S_{gm}} \tag{3}$$

Similarly, Figure 11 shows the water trapping model derived for near miscible and miscible WAG in rather oil-wet reservoir, consistent with extensions of classical trapping models to three-phase flow (Land [14], Shahverdi and Sohrabi [12]). The trapped water saturation, which is always higher than the initial water saturation, increases with the maximum water saturation reached during the preceding water slug (Swm). The correlation coefficient Cw plays a role analogous to the Land trapping coefficient: lower Cw values lead to higher trapped water saturation.

$$C_w = \frac{1}{S_{wt} - S_{wi}} - \frac{1}{S_{wm} - S_{wi}} \tag{4}$$

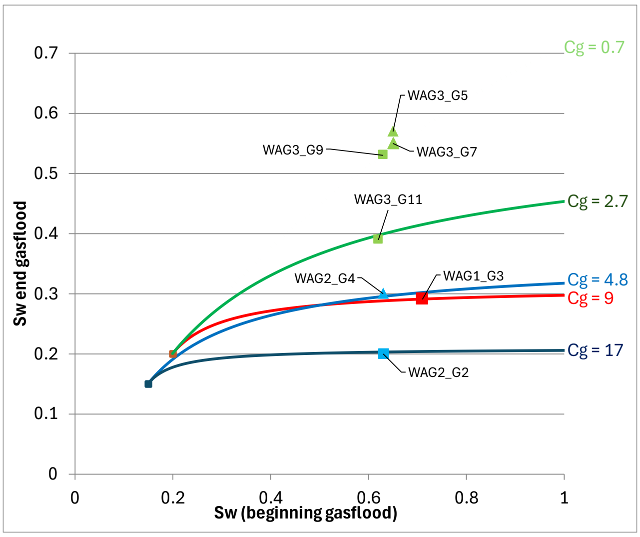

Figure 11 - *Estimation of Cw from WAG1A, WAG2 and WAG3 on the Swt/Swm plot. Symbols represent endpoint values derived from material balance, while solid lines correspond to the Land trapping model*

Figure 10 and Figure 11 are plotted in zero-dimensional SCAL approach, meaning they utilize the average core saturation. They provide a reliable estimate of the Cg and Cw values, which are essential for conducting the history match, where saturation levels vary along the core length.

The relationship observed between trapped gas saturation and maximum gas saturation is consistent with early three-phase WAG experiments, which demonstrated the fundamental role of gas trapping and hysteresis during cyclic water and gas injection (Skauge and Larsen, [4]).

The comparison of the injectivity index of the three WAG experiments presented in Puyou et al.[6] shows transient then steady-state effects. It demonstrates that the water stabilized the gas injection for quite some time. As expected, this effect partially vanished after long lasting continuous gas injection (end of chase gas).

Figure 12 illustrates the evolution of the water and gas injectivity indices for WAG1a experiment:

$$I.I._W = {Q_w . B_w}/_{\Delta P} \tag{5}$$

$$I.I._G = {Q_g . B_g}/_{\Delta P} \tag{6}$$

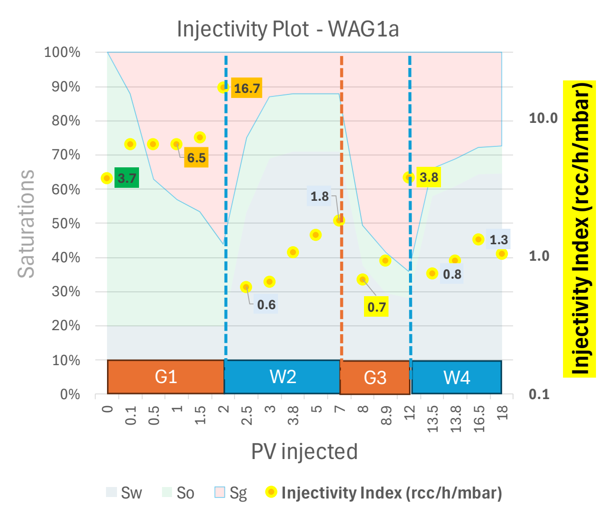

Figure 12 - *Injectivity index evolution for WAG1a during the cycle: gas injection (G1), water injection (W2), gas injection (G3) and water injection (W4)*

This injectivity index analysis confirms the existence of a gas mobility reduction during WAG cycles (G3), as described in cycle-dependent hysteresis models (Larsen and Skauge, [11]). In the present formulation, this effect is represented by the gas mobility reduction factor, αg, defined as the ratio between the effective gas mobility during WAG injection and that obtained under primary drainage conditions at comparable gas saturation. It is illustrated by Figure 13.

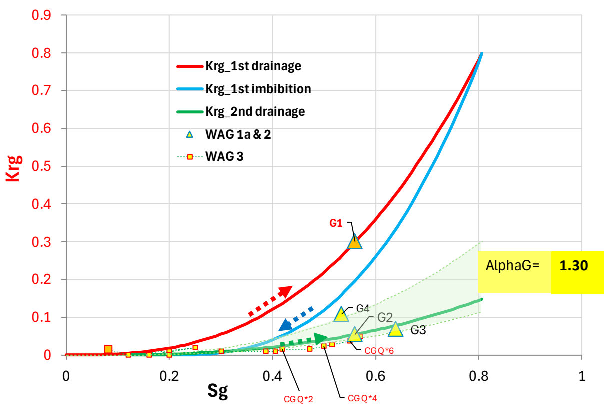

Figure 13 - *Estimation of α_g on Krg plot*

For a given imposed gas flow rate, αg can equivalently be expressed as the ratio of pressure gradients measured during continuous gas injection and during WAG gas injection. This formulation enables a purely experimental assessment of gas mobility reduction, integrating gas trapping and relative permeability hysteresis effects without requiring spatially resolved flow modeling.

The zero-dimensional SCAL approach results should not be considered quantitatively, as they are based on average data obtained from the core. Nonetheless, they offer valuable guidance for history matching by providing logical constraints for the relative permeability model. To achieve more precise results, interpretation through simulation and history matching of the experimental data is crucial.

5.5 Control of compositional exchanges

Near-miscible gas injection can lead to excessive oil vaporization when instantaneous equilibrium is assumed. Three mitigation strategies were tested: (i) a residual oil saturation (SOR) constraint limiting evaporation at the grid-cell scale, (ii) alpha-factor transport coefficients slowing down gas–oil compositional exchanges and (iii) binary interaction coefficients, introduced in EOS, mixing rules to account for non-ideal cross-interactions between dissimilar components. The coefficients were tuned against experimental phase-behavior data in order to properly reproduce vapor–liquid equilibria and miscibility conditions.

(i) SOR

Hydrocarbons are classified into "mobile hydrocarbons" and "residual oil". Residual oil is a distinct phase trapped in pores and does not flow or affect flash results. It is included in the total oil saturation, influencing Kr and Pc, but does not affect phase split or phase properties such as density and viscosity. Mobile oil is treated in a conventional manner.

Residual oil saturation in each cell is set to the minimum of the initial oil saturation and the value specified by the SOR keyword. Residual oil composition is equal to the initial oil composition in each cell. The number of residual moles stays constant throughout the simulation.

(ii) Alpha-factors

Alpha-factors are different from the WAG hysteresis parameter α_g. While α_g describes the reduction of gas mobility during cyclic WAG flow, alpha-factors are transport coefficients introduced in compositional simulation to account for sub-grid heterogeneity and non-equilibrium effects on coarse grids (Barker and Fayers, [18]). They are applied to component transport terms and are generally defined as mobility modifiers based on the concentration of a selected component, usually the main component of the injected gas.

In miscible and near-miscible gas injection, alpha-factors can also be used to limit excessive oil stripping during gas cycling. In coarse dynamic models, the local-equilibrium assumption may lead to complete vaporization of the oil in a gridblock, even though part of the oil remains bypassed and does not contact the injected gas. Alpha-factors help correct this effect by reducing instantaneous gas dissolution in oil at the coarse scale and by partly accounting for front instability effects such as fingering and channeling, which are not explicitly resolved on coarse grids (Barker et al., [19]; Bourgeois et al., [20]). Their use to preserve a realistic residual oil saturation during miscible and near-miscible gas flooding has been shown to improve the physical realism of compositional simulations.

(iii) Binary Interaction coefficient

Binary interaction parameters are widely used in EOS mixing rules to improve phase behavior predictions. In this study, they were adjusted to better reproduce the multi-contact miscible behavior observed during the WAG corefloods. The increase in differential pressure when gas enters the core suggests that gas/oil exchange is not instantaneous and that a finite interfacial resistance remains during displacement. Such behavior is not adequately reproduced by conventional compositional simulation under a strict local-equilibrium assumption. Sensitivity of Peng–Robinson predictions to binary interaction coefficients has also been highlighted for near-critical fluids (Slot-Petersen [21]).

This discrepancy is likely related to the instantaneous local equilibrium assumption inherent to compositional EOS, which may be valid at very small scales but is not supported by experimental observations at coreflood or reservoir flow rates.

Binary interaction coefficients provide a practical way to relax this assumption at the coarse scale. Originally introduced to improve phase behavior predictions in EOS mixing rules, they can also be used in upscaled models to account for non-ideal mass transfer and delayed equilibrium effects (Rios et al. [22]). As such, the BIC methodology, although primarily developed for 3D reservoir simulation, can be applied to 1D and 2D models to improve the reproduction of coreflood responses and enhance the consistency of history matching.

This method slows down the gas-oil interaction and a saturation gradient can be observed (Figure 14). With BIC methodology, the gas-oil transition is more representative as observed on 2D X-ray maps.

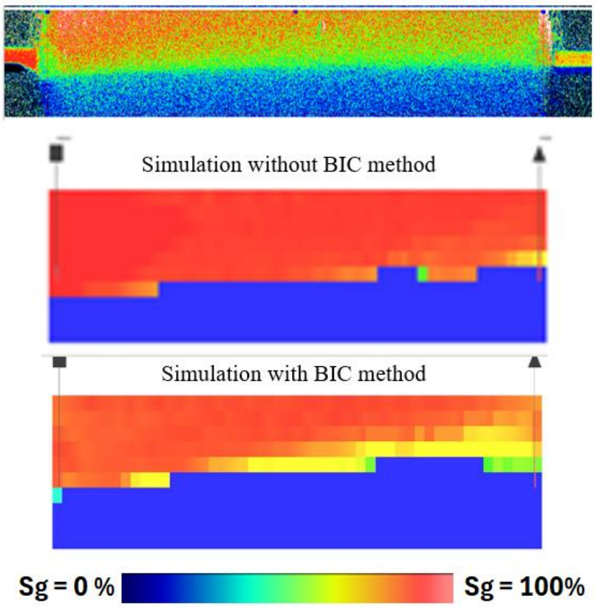

Figure 14 - *Comparison of 2D saturation gradient between X-ray measurement, conventional WAG hysteresis simulation and BIC methodology with the same color at t = 4h timestep.*

Degrading miscibility in compositional simulation has been proposed as an effective way to reproduce transport-limited gas–oil interactions observed experimentally (Bourgeois et al., [23]). Near-miscible WAG displacements involve both compositional oil stripping and interfacial tension effects, which cannot be captured using idealized miscible assumptions (Wang et al., [24]).

5.6 Multi-experiment consistency

A single, consistent parameterization framework (relative permeability, capillary pressure, and three-phase hysteresis parameters) was developed using the complementarity of the four corefloods, although the detailed history-match results presented in this paper focus on WAG1a. This experiment constrains gas-dominated flow and gravity effects, WAG2 constrains water-dominated flow and Pcow, WAG3 constrains true three-phase behavior within the ternary domain, and WAG1b isolates gravity-stabilized displacement. Parameter uncertainty was addressed through base, low, and high case ranges, all relying on the same unified parameterization framework rather than tuning individual experiments independently.

6 Results and discussion

Long-slug experiments WAG1a and WAG2 highlight the dominant impact of gravity segregation and injection sequence on sweep efficiency, with gas preferentially flowing at the top of horizontal cores. Alternating water injections stabilize the gas front and progressively improve vertical sweep. Gravity segregation and viscous instability effects observed in this study are consistent with recent experimental and numerical investigations of WAG displacement (Skauge et al., [25]).

WAG3 exhibits rapid injectivity stabilization, high sweep efficiency and controlled gas–oil interaction. Saturation trajectories plotted on a ternary diagram confirm that short slugs explore the central three-phase region more efficiently (Figure 1). This behavior is consistent with experimental observations showing that three-phase relative permeabilities can be significantly lower than two-phase values in low-IFT WAG systems (Sohrabi et al., [26]).

In this paper, only the history match of the WAG1a experiment is presented. The interpretation was performed using a two-dimensional grid to account for the strong segregation observed during displacement.

A comprehensive sensitivity analysis was conducted to evaluate different history matching strategies, including conventional, improved, and extended WAG hysteresis formulations, combined with SOR and alpha-factor approaches. In addition, the impact of binary interaction coefficients (BIC) was investigated using the improved WAG hysteresis model.

Simulation results were systematically compared to material balance estimates to assess the consistency and physical relevance of each approach and identify the most robust interpretation workflow.

6.1 History matches results

Simulation results were obtained using reservoir simulation software with the SOR, alpha-factors, BIC hypothesis and the three different WAG hysteresis scenarios alongside the material balance. These comparisons consider the assumptions for material balance calculations (Puyou et al.[6]), specifically focusing on oil saturations with Bo = Bc, where Bo is the oil reservoir and surface volume factor and Bc the equivalent for condensate:

$$RF_{surface.direct} = \frac{(V_{Oil@Lab}+V_{cond@Lab})}{STOOIP} \quad (7)$$

$$So_{surface\_direct} = Soi \cdot (1 - RF_{surface\_direct}) \quad (8)$$

$$Sw = Swi + (V_{injw@P,T} - V_{prodw@P,T}) / PV \quad (9)$$

$$Sg = 1 - So - Sw \quad (10)$$

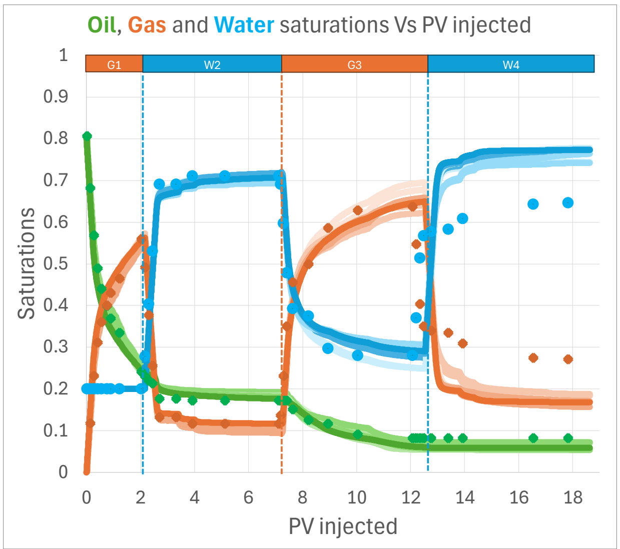

Figure 15 - *WAG1a Oil, gas and water saturation history match. solid lines represent the results obtained from various simulation scenarios (WAG hysteresis classic + SOR, WAG hysteresis Improved + SOR, WAG hysteresis Extended + SOR, WAG hysteresis Classic + Alpha-factors, WAG hysteresis Improved + Alpha-factors, WAG hysteresis Extended + Alpha-factors, WAG hysteresis Improved + BIC), while the dots correspond to the material balance calculations.*

Figure 15 compares simulated oil, gas, and water saturations against material balance results. Overall, all tested methodologies provide comparable quality match at the global scale, demonstrating their ability to reproduce the main displacement trends. However, differences emerge when analyzing phase behavior during cyclic injection.

In particular, the conventional WAG hysteresis formulation shows noticeable deviations in gas and water saturations at the end of the second gas injection cycle, mainly due to its limited ability to reproduce water trapping effects. This discrepancy persists during the final cycle, highlighting the limitations of the classical approach in capturing cycle-dependent hysteresis mechanisms.

In contrast, both the improved and extended WAG hysteresis models better reproduce the observed saturation dynamics, especially the progressive accumulation of trapped water. The incorporation of SOR and alpha-factors further enhances the consistency of the match by limiting excessive stripping and improving the representation of multi-contact miscible behavior at the grid scale.

BIC-based simulations were performed only with the improved WAG hysteresis formulation and lead to a similar overall match quality. They provide an alternative way to account for non-equilibrium effects, although no significant improvement was observed at the level of global saturation trends compared to the other advanced approaches.

6.2 Simplified cost function

To quantify the differences between history-matching methodologies, a normalized objective function was computed for each simulation case. The total cost function combines contributions from oil, water and gas saturations. Each contribution was normalized by the amplitude of the corresponding experimental signal at the end point of each cycle (G1, W2, G3) and avoiding the last cycle (W4). This representation allows a direct comparison of the different WAG hysteresis formulations and non-equilibrium correction methods (Figure 16).

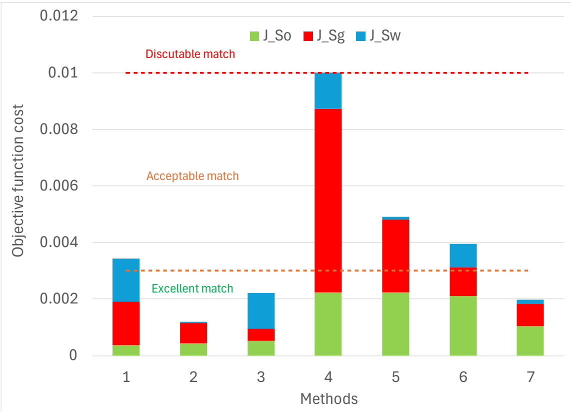

Figure 16 - *Normalized objective function for the different history-matching methodologies: (1) WAG hysteresis classic + SOR, (2) WAG hysteresis Improved + SOR, (3) WAG hysteresis Extended + SOR, (4) WAG hysteresis Classic + Alpha-factors, (5) WAG hysteresis Improved + Alpha-factors, (6) WAG hysteresis Extended + Alpha-factors, (7) WAG hysteresis Improved + BIC. Bars show the total mismatch, while colors indicate the contribution of each observable (oil, water, gas saturations).*

The normalized objective function confirms that all advanced formulations provide comparable global matches. However, significant differences are observed in the contribution of water and gas saturation mismatches. The conventional WAG hysteresis formulation leads to higher errors in gas and water saturations during later cycles, while improved and extended models reduce these discrepancies.

The use of SOR generally leads to lower objective function values and therefore to higher-quality matches in terms of global saturation behavior. However, it should be noted that the objective function used in this study is simplified and only accounts for saturation data, without including effluent composition data. This limitation does not fully capture the main advantage of alpha-factors, which are specifically designed to improve the representation of gas–oil compositional exchanges and stripping phenomena. Consequently, alpha-factors may offer additional benefits when composition data are included in the matching process, particularly for applications involving upscaling and field-scale simulations where non-equilibrium effects become more critical.

Finally, the BIC approach also provides satisfactory results, delivering a comparable match quality while offering an alternative way to account for non-equilibrium behavior through fluid model adjustments.

6.3 Synthesis of WAG1a results

Good overall matches are obtained with all tested methods. However, accurate gas and water saturation levels during the second gas injection (G3) require the inclusion of water trapping through the improved or extended WAG hysteresis formulations.

Conventional hysteresis models, based on a single set of parameters, often fail to simultaneously reproduce successive water injection cycles, particularly in terms of injectivity and pressure response. In this study, gas trapping was initially modeled using the classical Land formulation, which assumes a unique trapping coefficient (Cg) independent of cycle number and controlled solely by saturation history.

However, experimental data clearly exhibit cycle-dependent behavior, with progressive changes in gas mobility and water injectivity. This indicates that a single Land coefficient is insufficient to reproduce fully cyclic WAG processes. Although varying Cg between cycles could improve the match, this approach lacks physical justification and reduces model predictivity. The observed variations are more consistently explained by cumulative hysteresis effects, evolving phase connectivity, and changes in pore-scale fluid distributions.

As a result, cycle-dependent adjustment of Cg was not considered. In addition, the last injection cycle was not included in the matching process. Indeed, comparison with the WAG3 experiment—characterized by faster WAG cycles and more representative of field conditions—shows more consistent trends in water and gas saturation evolution (Figure 17).

This behavior suggests that the discrepancies observed in the final cycle of WAG1a are less representative of the underlying physical mechanisms governing field-scale displacement.

Overall, these results highlight the intrinsic limitations of conventional hysteresis models for cyclic WAG processes and support the use of more advanced formulations accounting for hysteresis memory and multi-cycle effects (Chen et al. [27]).

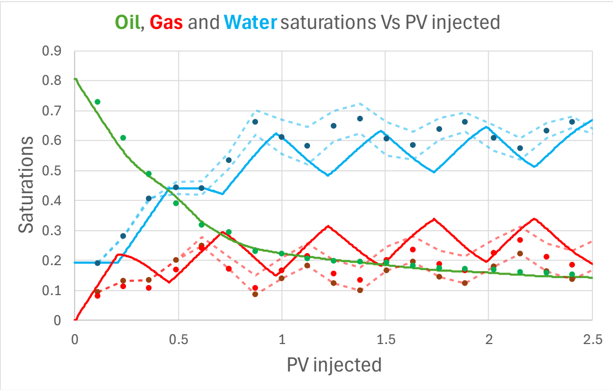

Figure 17 – *WAG3 Oil, gas and water saturation history match. solid lines represent the simulated results obtained with WAG hysteresis Improved + SOR, while the dots correspond to the material balance calculations with their uncertainty in dashed lines.*

Differential pressure discrepancy was globally observed due to gas-oil capillary pressure and higher water-oil capillary pressure from the second cycle that must be added to the simulation deck.

Pcgo and higher Pcow implementations were possible by representing dead volumes in the experiment without degrading saturation matches (Figure 18). Dead volumes added to the simulation help to stabilize results and reduced convergence issues in the simulation process.

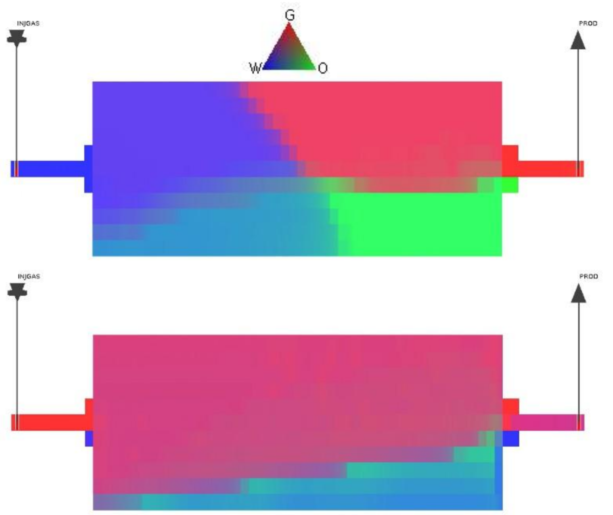

Figure 18 - *Oil, gas, water distribution during water injection (top image) and second gas injection (bottom image) - Good representativity of the gravity effects on first water injection in presence of gas and Second gas injection of WAG1a described by a 2D grid with the implementation of the inlet and outlet dead volumes*

In this high permeability environment, the differential pressure experimentally measured was very low. All the parameters influence the results. The representation of the dead volumes shows variability in accordance with the way they are represented in the simulation and with the parameters affected to them (permeability, Kr…).

Including all these hypotheses helps to obtain a correct match of the differential pressure as demonstrated in Figure 19.

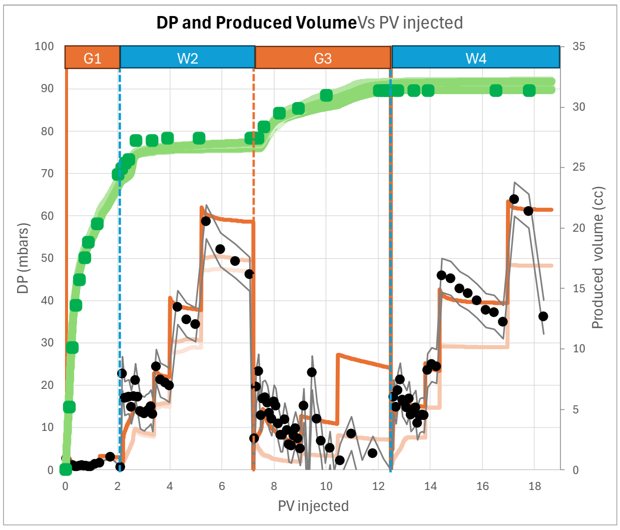

Figure 19 – *Differential pressure match with a 10 pseudo-components EOS and simulation of the inlet and outlet dead volumes*

Under the experimental conditions investigated for WAG1a, the WAG-hysteresis Improved formulation provided the most consistent match among the tested approaches. SOR-based simulations gave the lowest saturation-based objective function, whereas alpha-factors and BIC remain relevant complementary approaches for representing compositional exchanges and non-equilibrium effects, particularly in an upscaling perspective.

8 Conclusions

This study highlights the importance of selecting appropriate hysteresis formulations and non-equilibrium corrections to accurately reproduce cyclic WAG coreflood experiments (Figures 20 and 21).

While all advanced approaches provide satisfactory global matches, significant differences arise in their ability to capture gas and water saturation evolution, particularly during later cycles. Improved and extended WAG hysteresis formulations demonstrate a clear advantage over conventional models by better accounting for cumulative trapping effects and hysteresis memory.

The comparative analysis also shows that SOR-based approaches provide robust and consistent matches when focusing on saturation trends, whereas alpha-factors and BIC formulations offer complementary capabilities to better represent compositional exchanges and non-equilibrium effects. These latter approaches are particularly relevant when extending the analysis towards upscaling and field-scale applications.

Based on these results, a consistent interpretation workflow is proposed:

1) *Initial calibration of two-phase flow functions:*

Relative permeability (Kr) and capillary pressure (Pc) are first constrained using the initial injection slugs (water for oil–water Kr, gas for gas–oil Kr) from long-slug experiments such as WAG1a and WAG2.

2) *Identification of three-phase parameter ranges:*

Sensitivity analyses are performed in a simplified (0D) framework to define realistic ranges for key three-phase parameters (Cg, αg, Rkw, Cw, Swt).

3) *Core-scale history matching:*

Simulations are performed using the WAG hysteresis improved formulation combined with the SOR approach, providing a robust baseline match of saturation behavior.

4) *Extension to advanced formulations for upscaling:*

More advanced approaches such as alpha-factors or BIC are then introduced to better capture compositional effects and non-equilibrium behavior, particularly in the perspective of field-scale simulation and upscaling studies.

This workflow provides a structured and physically consistent approach for interpreting WAG coreflood experiments, while ensuring a clear transition from laboratory-scale calibration to reservoir-scale modeling.

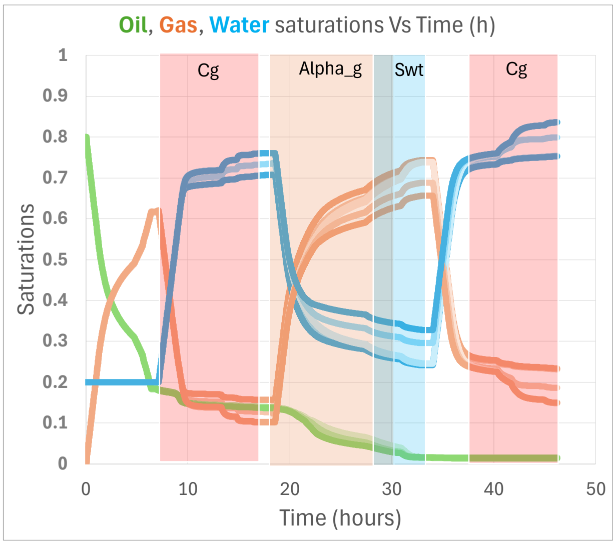

Figure 20 - *Impact of WAG hysteresis three-phase parameters. Single-parameter sensitivity analysis performed using the WAG hysteresis improved formulation, without SOR, Alpha-factors or BIC.*

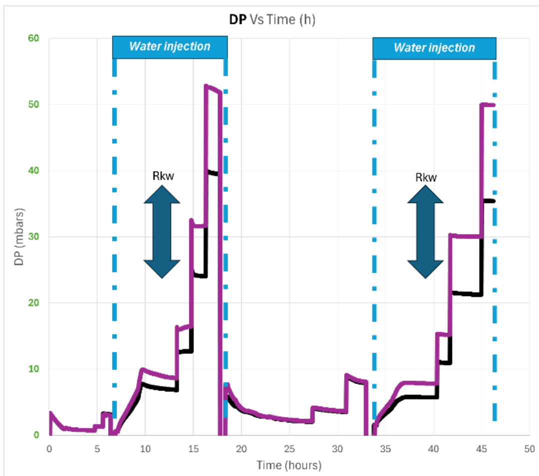

Figure 21 – *Effect of the Rkw parameter on differential pressure response.*

Nomenclature

α_g = Gas mobility reduction parameter
BIC = Binary interaction coefficients
Bo, Bc = Oil and condensate reservoir to surface ratio
Cg, Cw = Gas and water Land parameter
EOS = Fluid Equation of State
HPHT = High Pressure High Temperature
$I.I._W$, $I.I._G$ = Water and gas injectivity index
IX = Intersect reservoir simulator
Kr = Relative permeability
Krw, Krg, Kro = Water, gas, oil relative permeability
Pc = Capillary pressure
Pcow, Pcgo = Water-oil, gas-oil capillary pressure
PV = Pore Volume
RF = Recovery factor
Rkw = Reduction of water relative permeability
SCAL = Special core analysis
So, Sw, Sg = Oil, water, gas saturation
SOR = IX keyword for residual oil saturation
STOOIP = Stock tank oil originally in place
WAG = Water alternating gas

Acknowledgements

The authors would like to thank TotalEnergies, APA Corporation and Staatsoilie Maatschappij for granting permission to publish this work. The authors also gratefully acknowledge the support and collaboration of the members of the integrated project team: Vincente Onwuchekwa, Michael Hunter, Karuna Bhoendie, Joaquin Osses-Fiorentino, Yoann Guilloux.

References

1. P. Egermann, M. Robin, J.-M. Lombard, Gas process displacement efficiency comparisons on a carbonate reservoir, SPE-81577 (2003)
2. J.O.S. Pizarro, et al., Optimizing production of Santos Basin pre-salt fields through sound reservoir management practices, OTC-27993 (2017)
3. L. Burns, et al., Guyana: Liza Phase 2 novel execution to accelerate field development, OTC-30948 (2021)
4. Skauge, J.A. Larsen, Three-phase relative permeabilities and trapped gas measurements related to WAG processes, SCA 9421 (1994)
5. M. Bourgeois, Recent importance of gas-based EOR, EAGE Proceedings (2025), https://doi.org/10.3997/2214-4609.2025101529
6. G. Puyou, M. Bourgeois, B. Satken, Gas–oil interaction and gravity impact on high permeability WAG experiments, SCA-1039 (2025)
7. S. Duchenne, R. de Loubens, M. Petitfrère, T. Joubert, Modeling and simultaneous history-matching of multiple WAG coreflood experiments at reservoir conditions, SPE-177531 (2015)
8. T. Joubert, S. Duchenne, M. Bourgeois, R. de Loubens, M. Petitfrere, Experimental data acquisition and modeling for the study of miscible CO_2 WAG in carbonate reservoirs under oil-wet conditions, SPE-188471 (2017)
9. S. Savin, M. N'Guyen, G. Puyou, CXBOX: An innovative tool for fluid dynamic quantification during corefloods, SCA037 (2017)
10. J.E. Killough, Reservoir simulation with history-dependent saturation functions, SPE J. 16, 37–48 (1976), https://doi.org/10.2118/5106-PA
11. J.A. Larsen, A. Skauge, Methodology for numerical simulation with cycle-dependent relative permeabilities, SPE J. 3, 163–173 (1998), https://doi.org/10.2118/38456-PA
12. H. Shahverdi, M. Sohrabi, An improved three-phase relative permeability and hysteresis model for the simulation of a water-alternating-gas injection, SPE-152218 (2013)
13. M. Bourgeois, B. Satken, P. Goyal, S. Saeed Al Eissaee, C. Cottin, E. Draoui, Using WAG laboratory data to derisk water injection at the gas-oil contact on a giant offshore field, SPE-221899-MS (2024)
14. C.S. Land, Calculation of imbibition relative permeability for two- and three-phase flow from rock properties, SPE J. 8, 149–156 (1968), https://doi.org/10.2118/1942-PA
15. L. Heidari, V. Gervais, M. Le Ravalec, H. Wackernagel, History matching of reservoir models by ensemble Kalman filtering: The state of the art and a sensitivity study, AAPG Mem. 96, 249–264 (2011)
16. S. Duchenne, G. Puyou, P. Cordelier, J. Hy-Billiot, G. Hamon, Efficient experimental data acquisition for miscible CO_2 WAG injection corefloods in carbonate, SPE-169045 (2014)
17. P. Mahzari, M. Sohrabi, An improved approach for estimation of flow and hysteresis parameters applicable to WAG experiments, SPE-183321-MS (2016), https://doi.org/10.2118/183321-MS
18. J.W. Barker, F.J. Fayers, Transport coefficients for compositional simulation with coarse grids in heterogeneous media, SPE Advanced Technology Series 2, 103–112 (1994), https://doi.org/10.2118/22591-PA
19. J.W. Barker, M. Prévost, E. Pitrat, Simulating residual oil saturation in miscible gas flooding using alpha-factors, SPE-93333-MS (2005), https://doi.org/10.2118/93333-MS
20. M. Bourgeois, S. Thibeau, J. Guo, Modelling residual oil saturation in miscible and immiscible gas floods by use of alpha-factors, SPE-143379 (2011)
21. Slot-Petersen, A systematic and consistent approach to determine binary interaction coefficients for the Peng–Robinson equation of state, SPE Reservoir Engineering 4, 488–494 (1989), https://doi.org/10.2118/16941-PA
22. V.S. Rios, O.S. Santos, F.B. Quadros, D.J. Schiozer, New upscaling technique for compositional reservoir simulations of miscible gas injection, J. Petrol. Sci. Eng. 175, 389–406 (2019), https://doi.org/10.1016/j.petrol.2018.12.061
23. M. Bourgeois, M. Hunter, C. Le Goff, N. Lindeloff, Investigation of methodology to degrade miscibility in compositional simulation, EAGE Proceedings (2025), https://doi.org/10.3997/2214-4609.202531054
24. G. Wang, G. Pickup, K. Sorbie, E. Mackay, A. Skauge, Analysis of near miscible CO_2 WAG displacements: The distinction between compositional and interfacial tension effects, SPE-193907 (2019)
25. Skauge, T. Skauge, K. Sorbie, M. Bourgeois, Impact of viscous instabilities on WAG displacement, SPE-211448 (2022)
26. M. Sohrabi, H. Shahverdi, M. Jamiolahmady, M. Fatemi, S. Ireland, G. Robertson, Experimental and theoretical three-phase relative permeability for WAG injection in mixed-wet and low-IFT systems, SCA2010-09 (2010)
27. Y. Chen, S. Wu, D. Zhou, A. Chawathe, A. Inouye, Impact of relative permeability hysteresis on water-alternating-gas injectivity: Modeling and experimental study, SPE-187425 (2017), https://doi.org/10.2118/187425-MS